Corresponding Author Dashboard

3 Manuscripts I Have Co-Authored

Start New Submission

Legacy Instructions

5 Most Recent E-mails

Manuscripts I Have Co-Authored

STATUS	ID	TITLE	CREATED	SUBMITTED
Contact Journal ADM: ASTM Editorial, Emily Dye and Victoria Lambert • A- Accept as is (05-Dec-2024)	JTE-2024-0210.R1	Evaluation of damage and nonlinearity of cold recycled materials mixtures using a new strain sweep testing procedure View Submission Submitting Author: Graziani, Andrea Cover Letter	17-Jul-2024	24-Jul-2024

Journal of Testing and Evaluation

Evaluation of damage and nonlinearity of cold recycled materials mixtures using a new strain sweep testing procedure

Journal:	*Journal of Testing and Evaluation*
Manuscript ID	JTE-2024-0210.R1
Manuscript Type:	Technical Manuscript
Date Submitted by the Author:	24-Jul-2024
Complete List of Authors:	Grilli, Vittoria; Università Politecnica delle Marche, Department of Civil and Building Engineering and Architecture Graziani, Andrea; Università Politecnica delle Marche, Department of Civil and Building Engineering and Architecture Virgili, Amedeo; Universita Politecnica delle Marche, Department of Civil and Building Engineering and Architecture Jaczewski, Mariusz; Gdansk University of Technology, Transportation Engineering Department
ASTM Committees and Subcommittees:	D04.99 Sustainable Asphalt Pavement Materials and Construction < D04 ommittee on Road and Paving Materials
Keywords:	Cold recycling, Cement-bitumen-treated materials, Stiffness modulus, Strain sweep, Damage, Nonlinearity, Dissipated energy

This is an article accepted for publication in Journal of Testing and Evaluation, Copyright © 2025, ASTM International, West Conshohocken, PA, DOI: 10.1520/JTE20240210

Evaluation of damage and nonlinearity of cold recycled materials mixtures using a new strain sweep testing procedure

Vittoria Grilli[1], Andrea Graziani[2(*)], Amedeo Virgili[3] and Mariusz Jaczewski[4]

ABSTRACT

This paper describes a new strain sweep testing method to identify the effects of damage and reversible nonlinearity. Indirect tensile stiffness modulus tests were performed at increasing strain (up to 322 με) to evaluate the stiffness behavior with increasing damage, in parallel tests at small strain (43 με) were performed to evaluate the linear behavior. Tests were carried out on two cement-bitumen-treated materials (CBTM) mixtures produced in Italy and Poland. Two asphalt concrete (AC) specimens extracted from a Polish road were also tested for comparison. Results were analyzed separately for the steps of increasing strain, and the steps at small- strain. Two approaches were used in the analysis: one was based on the resilient stiffness modulus; the other was based on the dissipated energy. The results showed that both approaches allowed to separate the effects due to nonlinearity from those due to damage in both CBTM and AC mixtures. Moreover, the damage evolution on CBTM mixtures was not affected by the testing temperature and the mixture composition.

[1] Department of Civil and Building Engineering and Architecture, Università Politecnica delle Marche, via Brecce Bianche, Ancona, Italy, ORCID: 0000-0002-2429-2699

[2] (*) **Corresponding Author, a.graziani@univpm.it** Department of Civil and Building Engineering and Architecture, Università Politecnica delle Marche, via Brecce Bianche, Ancona, Italy, ORCID: 0000-0003-3796-9694

[3] Department of Civil and Building Engineering and Architecture, Università Politecnica delle Marche, via Brecce Bianche, Ancona, Italy, ORCID: 0000-0001-7679-7456

[4] Transportation Engineering Department, Faculty of Civil and Environmental Engineering, Ekotech Center, Gdansk University of Technology, Gdansk, Poland, ORCID: 0000-0003-4722-2957

Keywords: Cold recycling, cement-bitumen-treated materials, stiffness modulus, strain sweep, damage, nonlinearity, dissipated energy.

Introduction

Cold recycling of bituminous pavements is currently one of the most environmentally friendly and cost-effective technologies for reconstruction of old roads[1-5]. It allows to maximize the reuse of reclaimed asphalt pavement (RAP), often containing tar, without using high temperatures. Cold recycled material (CRM) mixtures are produced using bitumen (in the form of emulsion or foam) and supplementary binder (usually cement). The dosage of binders is determined by the requirements of specific location or country and differ strongly[1,3,6-8]. A commonly used family of CRM mixture is cement-bitumen-treated materials (CBTM)[9], which is characterized by a dosage of cement between 1.5% and 4.0% and a dosage of emulsion between 2.0 and 6.0 %. CBTM mixtures typically show a thermo-viscoelastic behavior similar to that of hot-mix asphalt, and their load-related failure is primarily in fatigue[10,11]. However, both the fatigue and the thermo-viscoelastic behavior of CBTM mixtures strongly depend on the dosage binders, especially cement.

Test procedures developed primarily for hot-mix asphalt are utilized also for characterizing CRM mixtures, normally without changing any assumption or setting; a typical example is the indirect tensile test. In specifications for designing CRM mixtures, very often indirect tensile strength and indirect tensile stiffness modulus are utilized as base indicators. In Europe, for example, the indirect tensile stiffness modulus test is routinely carried out following the EN 12697-26 (Annex C, IT-CY) that recommends values of the maximum horizontal deformation comprised between 2.5 μm (at -5 °C) and 9.0 μm (at 25 °C). In the case

of CRM mixtures, typical values assumed in the literature[12], for specimens with 100 mm diameter, are in the range of 2 μm to 7 μm. Polish and German specifications suggest that the target horizontal deformation value should be 5 μm for testing at 5 ˚C.

Often, it is implicitly assumed that the linearity limits[13] of hot-mix asphalt and CRM mixtures are the same. However, recent research has shown that the stiffness modulus determined in cyclic compression test for CRM mixtures is strongly dependent on the applied strain[14,15], even at amplitudes below 50 με. Moreover, by using the IT-CY test with increasing and decreasing deformation levels[12], it was clearly shown that damage appears even at deformation levels as low as 6 μm. Such behavior is not present in hot-mix asphalt.

For hot-mix asphalt, increasing stress/strain beyond the linearity limit leads to a decreasing of stiffness modulus and an increasing of phase angle[16,17]. Those changes initially include both reversible (nonlinear) and irreversible (damage) effects. At higher values of stress/strain damage prevails, eventually leading to failure. Moreover, testing at strain levels exceeding the linearity limit, using strain sweep test protocols, has been proposed to estimate the fatigue life of both bituminous binders[18] and hot-mix asphalt mixtures[19,20,21].

The behavior of CRM mixtures is different and affected by both the composition of the mixture and the type of test. In cyclic compression tests[5], CRM mixtures did not show a linear behavior with increasing strain. In particular, the modulus values changed with two rates of change, up to around 100 με (higher rate) and above 100 με (lower rate). However, all the changes were reversible (nonlinear behavior), even in the highest test temperature of 40 °C. Preliminary tests on CRM mixtures with the IT-CY test scheme[12] showed a similar behavior with increasing horizontal deformation. In this case however the stiffness reduction was only partially reversible, and, in some cases, specimens showed damage with strong and irreversible

decrease of the measured stiffness modulus. Analogous results were observed in multi-step and multi-round stiffness tests conducted using an indirect tensile configuration on CRM mixtures with foamed bitumen[22,23]. These tests revealed that the resilient stiffness was influenced by the maximum strain level, or more precisely, by the extent of damage the material had already sustained. However, after repeated loading, the resilient stiffness of the CRM mixtures stabilized and remained nearly constant.

The main outcome of the past studies was that the effect of strain level on the stiffness behavior CRM mixtures needs more detailed investigation. A standardized method is needed to identify nonlinearity and damage effects, and if there is any limit after which one of those effects prevails. Also, a standardized method is also needed to evaluate whether factors such as temperature, type and dosage of binding agents, and mixture composition affect the deformation-related behavior.

The objective of the present research is to describe a new testing procedure for evaluating damage accumulation in CBTM mixtures, separating the irreversible effects from reversible effects due to nonlinearity. The procedure is based on indirect stiffness modulus tests performed at increasing deformation levels and, in parallel, at small deformation. Asphalt concrete (AC) specimens were also tested for comparison. The experimental work was carried out at Università Politecnica delle Marche (UNIVPM), on a typical Italian mixture, and at Gdansk University of Technology (GUT), on typical Polish mixtures.

Materials

Three different mixtures were tested in this study: two CBTM mixtures and one AC mixture. The first CBTM mixture was produced at UNIVPM using 80 % (by aggregate mass)

of RAP with a nominal maximum size of 16 mm, and 20 % of limestone filler. The dosages of binders were 4.0 % (by aggregate mass) of modified bitumen emulsion, designated as C60BP10 (EN 13808) produced with 60 % residual bitumen 70/100, and 2.0 % of Portland limestone cement designated as CEM II/A-LL 42.5 R (EN 197-1). The total water content of the mixture was 4.5 % (by aggregate mass), including emulsion water and pre-wetting water. Cylindrical specimens with nominal diameter of 100 mm and height of 70 mm were produced using a gyratory compactor by applying a constant pressure of 600 kPa, a rotation speed of 30 rpm, and an angle of inclination of 1.25˚. The target void level was 14 %. Six specimens were compacted, two replicates for three test temperatures. The compacted specimens were immediately extracted from the mold and cured at 40 °C and 70 % relative humidity for 28 days before testing.

The second CBTM mixture was produced at GUT using 67 % (by aggregate mass) of RAP with a nominal maximum size of 31.5 mm, and 33 % of natural aggregate including two fractions: 0/4 (34%) and 0/16 (66%). The dosages of binders were 5.5 % (by aggregate mass) of bitumen emulsion, designated as C60B10 (EN 13808) produced with 60 % residual bitumen 70/100, and 3.0 % of Portland fly-ash cement designated as CEM II/B-V 32.5 R (EN 197-1). The total water content of the mixture was 6.0 % (by aggregate mass), including emulsion water and pre-wetting water. Cylindrical specimens with nominal diameter of 101±2.0 mm and height of 63.5 ±3.5 mm were produced using a perforated Marshall mold, with 75 blows for each face. The target void level was 14 %. The compacted specimens were immediately extracted from the mold and cured at 20 °C and 70 % relative humidity for 28 days before testing. Three replicate specimens were tested.

The AC specimens were obtained from the pavement of one of national road in Poland. The mixtures were designed, and the pavement of the national road was constructed according to Polish requirements WT-2 2014 and WT-2 2016. The tested material was produced using limestone filler and natural fine and coarse aggregate (gneiss/granodiorite) with a nominal maximum size of 22 mm. The dosage of binder was 4.0 % (by aggregate mass) of non-modified bitumen, designated as 35/50 (EN 13108). Cylindrical specimens with nominal diameter of 100 mm and height of 47.0±2.0 mm were cut from cores. As the pavement was not a dedicated field section, its construction was performed in typical conditions. The target void level was 7 %. Two replicate specimens were obtained for laboratory testing.

Table 1 lists the main physical properties of the tested specimens.

TABLE 1. Main physical properties of the specimens involved in this study.

Specimen ID	Cement (%)	Bitumen (%)	Height (mm)	Target voids (%)	Test temperature (˚C)
CBTM_R1_I	2.0	2.4	70.0	14.0	5
CBTM_R2_I	2.0	2.4	70.0	14.0	5
CBTM_R3_I	2.0	2.4	70.0	14.0	20
CBTM_R4_I	2.0	2.4	70.0	14.0	20
CBTM_R5_I	2.0	2.4	70.0	14.0	35
CBTM_R6_I	2.0	2.4	70.0	14.0	35
CBTM_R1_P	3.0	3.3	62.0	14.0	20
CBTM_R2_P	3.0	3.3	62.6	14.0	20
CBTM_R3_P	3.0	3.3	63.2	14.0	20
AC_R1_P	-	4.0	46.7	7.0	20
AC_R2_P	-	4.0	47.6	7.0	20

Methods

The proposed test method consists in consecutive indirect tensile stiffness tests performed along one diameter, at different levels of target horizontal deformation. A rest period of 5 min was allowed between two consecutive tests, to allow recovery of delayed deformation and to avoid heating effects.

Each test was performed according to the European standard EN 12697-26 Annex C (IT-CY). Loading pulses had a target rise time of 0.124 s and a repetition period of 2 s (in the case of Italy) or 3 s (in the case of Poland). The peak load values were determined by the dedicated program to achieve the target peak horizontal deformations listed above. The deformation was measured using two LVDTs sensors. Tests were carried out at temperatures of 5, 20, 35 ˚C for specimens tested in Italy, and at temperature of 20 ˚C for specimens tested in Poland. The tensile stress and strain at the center of the specimen were calculated as presented in the EN standard:

$$\sigma_0 = \frac{2F}{\pi \cdot t \cdot D} \quad (1)$$

$$\varepsilon_0 = \frac{2\,z}{D} \cdot \left[\frac{1 + 3\nu}{4 + \pi \cdot \nu - \pi}\right] \cdot 10^6 \quad (2)$$

Where F is the peak load, z is the peak horizontal deformation, t and D are the thickness and the diameter of the specimens, and ν is the Poisson's ratio value (assumed equal to 0.20). The resilient stiffness modulus was calculated as follows:

$$E = F \cdot \frac{(\nu + 0.27)}{z \cdot t} \quad (3)$$

It should be noted that equations (1), (2) and (3) are valid when the behavior of the material is linear. Since in this study nonlinearity and damage are investigated, E could not be

strictly defined. For this reason, the stiffness modulus obtained from the test can be considered as an "equivalent" stiffness modulus[24].

In the proposed strain sweep test procedure, the target peak horizontal deformation was increased from 2 μm to 15 μm, in steps of 1 μm. To check the damage induced to the specimens, tests were also performed at target horizontal deformation of 2 μm. Fig. 1 shows the complete strain sweep test procedure applied each sample.

FIGURE 1. Deformation and strain levels applied to the specimens and test pulses.

Results and analysis

RESULTS

Fig. 2 shows, as an example, the recorded time-histories of vertical force and horizontal deformation during the five test pulses at target deformations of 4 μm and 14 μm applied on two specimens: CBTM_R3_P and AC_R1_P. As it can be observed, the deformation curves were almost perfectly superposed, in both small and large deformation tests suggesting that the effect of cycle repetition was negligible.

The average stress and strain values in five test pulses were used for the Lissajous plots shown in Fig. 3. For the specimen CBTM_R3_P, Figure 3a shows the cycles obtained at increasing strain levels of 86, 215 and 322 με, whereas Figure 3b shows the three cycles obtained at 43 με, right after the cycles performed at strain levels of 86, 215 and 322 με. Figure 3c and 3d show the same plots for the specimen AC_R1_P. It can be observed that, for the CBTM mixture, as the strain level increased, the slope of the loading branch decreased at both

high (Fig. 3a) and small (Fig. 3b) strain levels. This indicates that the stiffness of the material is progressively reducing.

For the AC specimen the slope of the loading branch remained almost constant (Fig. 3c and 3d), indicating that the stiffness reduction suffered by the specimen is much less in comparison to the CBTM mixture.

FIGURE 2. Time-histories of five test pulses of vertical force and horizontal deformation, recorded on two specimens at target horizontal deformations of 4 μm and 14 μm; a) specimen CBTM_R3_P; b) specimen AC_R1_P.

FIGURE 3. Lissajous plots (stress vs strain) recorded at large and small strain: a) specimen CBTM_R3_P from 86 to 322 με; b) specimen CBTM_R3_P 43 με; c) specimen AC_R1_P from 86 to 322 με; d) specimen AC_R1_P 43 με.

Fig. 4 shows the values of E (average of the five test pulses) obtained for specimens CBTM_R3_P and AC_R1_P, as a function of the applied strain. A similar behavior was observed in all tested specimens. As it can be seen, in both cases the stiffness of the specimens decreased when the strain was increased. Each time the applied strain was reduced to 43 με, corresponding to a deformation of 2 μm, the recovery in E was partial, indicating that the specimen had been damaged. As outlined above this effect was more evident in specimen CBTM_R3_P. Furthermore, the values of E measured at 43 με reduced as the maximum strain applied to the specimen increased, indicating that the specimens were experiencing an increasing level of damage.

FIGURE 4. Resilient stiffness modulus measured in the strain sweep tests; a) specimen CBTM_R3_P; b) specimen AC_R1_P.

Fig. 5a shows the values of E measured only during the increasing steps of applied strain, which also correspond to the maximum strain level applied to the specimen. We designate these curves as "virgin" curves. The virgin curves obtained on five specimens of each analyzed material were plotted. For the same specimens, Fig. 5b shows the values of E measured at 43 με as a function of the maximum strain level previously applied to the specimen, i.e. at the previous strain step (Fig. 1). We designate these curves as "small-strain" curves.

In the semi-logarithmic plane, both the virgin and the small-strain curves follow well-defined linear trends that were fitted using an exponential equation:

$$E = E_0 \exp(-k\varepsilon) \quad (4)$$

where ε is the maximum strain applied to the specimen, E_0 is the resilient stiffness modulus at "zero deformation" and k is the slope of the line that characterizes the strain-dependance. The estimated values of E_0 and k for the virgin and small strain curves are summarized in Table 2.

FIGURE 5. Resilient stiffness modulus variation as a function of applied strain level: a) virgin curve; b) small-strain curve.

TABLE 2. Least-squares estimates of the parameters of Equation 4.

Specimen ID	k_V (-)	k_{SS} (-)

	$E_{0,V}$ (MPa)	$E_{0,SS}$ (MPa)	$E_{0,V}/E_{0,SS}$		
	Virgin	Small strain	(-)	Virgin	Small strain
CBTM_R1_I	7080	7578	0.934	$4.9 \cdot 10^{-3}$	$5.2 \cdot 10^{-3}$
CBTM_R2_I	8267	8329	0.992	$4.2 \cdot 10^{-3}$	$3.8 \cdot 10^{-3}$
CBTM_R3_I	5434	5389	1.008	$4.3 \cdot 10^{-3}$	$4.0 \cdot 10^{-3}$
CBTM_R4_I	7031	7344	0.957	$4.4 \cdot 10^{-3}$	$4.0 \cdot 10^{-3}$
CBTM_R5_I	5366	5370	0.999	$5.1 \cdot 10^{-3}$	$4.7 \cdot 10^{-3}$
CBTM_R6_I	5251	5000	1.050	$4.6 \cdot 10^{-3}$	$3.8 \cdot 10^{-3}$
CBTM_R1_P	5567	5818	0.956	$4.3 \cdot 10^{-3}$	$4.5 \cdot 10^{-3}$
CBTM_R2_P	5106	5121	0.997	$4.5 \cdot 10^{-3}$	$3.8 \cdot 10^{-3}$
CBTM_R3_P	4721	4597	1.026	$3.6 \cdot 10^{-3}$	$2.9 \cdot 10^{-3}$
AC_R1_P	8827	8904	0.991	$1.1 \cdot 10^{-3}$	$1.1 \cdot 10^{-3}$
AC_R2_P	7744	7598	1.019	$0.9 \cdot 10^{-3}$	$0.3 \cdot 10^{-3}$

For the CBTM specimens produced and tested in Italy, higher values of E were obtained at lower temperatures, at all strain levels (Fig. 5). The values of E measured on the CBTM specimens tested in Poland (only at 20 °C) were slightly higher but showed a very similar decreasing trend. For the AC specimen, the decreasing trend is similar, but the values of E are higher, and the slope is lower, compared to the CBTM mixtures.

The values of E_0 estimated from the virgin curve ($E_{0,V}$) and the corresponding small-strain curve ($E_{0,SS}$) were almost identical, in fact, their ratio was comprised between 0.95 and 1.05 (Tab. 2). This suggests that difference between $E_{0,V}$ and $E_{0,SS}$ was negligible, indicating that a unique E_0 value can be assumed as the limiting value of stiffness in the linear domain, when the specimen is not damaged.

The values of k are similar for two CBTM mixtures and comprised between 0.0036 and 0.0051 for the virgin curve (k_V) and between 0.0029 and 0.0052 for the small-strain curves (k_{SS}). The values of k estimated for AC were lower. Moreover, for both CBTM and AC, k_V was in almost all cases higher than k_{SS}. In fact, the values of E measured at the increasing strain levels

(virgin curves) are affected by both nonlinearity and damage effects. On the other hand, the values of E measured at 43 με (small-strain curves) were not affected by nonlinearity effects.

ANALYSIS IN TERMS OF DAMAGE

Fig. 6 shows the values of E/E_0 as a function of the maximum strain level applied to the specimen. For the three families of specimens, the average values were reported separately in the virgin and small-strain curves. The curves obtained from the CBTM specimens were almost perfectly superposed, regardless of test temperatures and different composition of the mixture. For the AC specimens the values of E/E_0 were higher, and the slope was lower, compared to the CBTM mixtures.

FIGURE 6. Normalized stiffness modulus versus maximum strain level: a) virgin curves; b) small-strain curves.

Figure 7 describes the proposed interpretation to separate damage from nonlinearity effects. The plots show the virgin curve and small-strain curve for specimens CBTM_R3_P and AC_R1_P, respectively. For the CBTM specimen, the virgin curve, affected by both nonlinearity and damage effects, was clearly below the small-strain curve, that is affected only damage effects. For the AC specimen, the virgin curve and small-strain curve were superposed, suggesting that the contribution of nonlinearity is negligible, with respect to damage. The small-strain curve proves to be a valuable tool for characterizing stiffness reduction due to damage. It is highlighted that other parasitic effects, like heating and thixotropy, should not be relevant because of the rest time between two tests at different strain levels.

FIGURE 7. Virgin and small-strain curves. a) specimen CBTM_R3_P; b) specimen AC_R1_P.

We can introduce a damage parameter D, defined as follows[25]:

$$D = 1 - \frac{E}{E_0} \tag{5}$$

where E and E_0 are the damaged and undamaged values of the stiffness modulus, respectively. When D is applied to analyze fatigue tests carried out at constant strain, the value of E is a function of the number of cycles, and E_0 is the initial value. In most cases, reversible phenomena such as heating and thixotropy, that occur during fatigue tests, are coupled with damage. In this research, we assume that E is a function only of the maximum strain level to which the specimen has been subjected during the test, whereas E_0 is the value estimated at "zero deformation" (Table 2). Therefore, we neglect the effect of load cycles repetition because of the low number of applied cycles (compared to classical fatigue tests) and because of the adopted rest times[12].

Comparing Equation 5 to Equation 4, it is possible to fit the curves in Fig. 6 with an exponential equation characterized by the same k values obtained above (Table 2). Consequently, the evolution law of D as a function of strain level can be expressed as follows:

$$\frac{\mathrm{d}D}{\mathrm{d}\varepsilon} = k \exp(-k\varepsilon), \qquad \text{with } \mathrm{d}\varepsilon > 0 \tag{6}$$

Virgin curves were affected by non-linearity, and thus the values of k_{SS} obtained for the small-strain curves provided a better characterization of damage evolution.

ANALYSIS IN TERMS OF DISSIPATED ENERGY

The dissipated energy per volume, per cycle (W) was calculated through the direct integration of the Lissajous plots (Fig. 3):

$$W = \frac{1}{2}\sum_{k=1}^{N}(\sigma_k + \sigma_{k-1}) \cdot (\varepsilon_k - \varepsilon_{k-1}) \quad (7)$$

where σ_k and ε_k are stress and strain samples measured during each cycle, and N is the total number of samples in one cycle. Fig. 8 shows the typical evolution of W as a function of the maximum strain level, for virgin and small-strain curves. Along the virgin curve (Fig. 8a) the applied strain increased, therefore W also increased. On the other hand, on the small strain-curve, the applied strain was constant, and W decreased because the specimens were affected by an increasing level of damage. It is highlighted that for the AC specimen (AC_R1_P), the values of W were higher, but the slope of the curve was lower, with respect to CBTM specimens.

FIGURE 8. Dissipated energy per volume, per cycle: a) virgin curves; b) small-strain curves.

For purely linear viscoelastic behavior i.e., when stress and strain are sinusoidal, the dissipated energy is calculated as follows[25].

$$W = \pi\sigma_0\varepsilon_0 \sin\varphi = \pi\varepsilon_0^2 E'' \quad (8)$$

where σ_0 and ε_0 are the amplitudes of the sinusoidal waves, φ is the phase angle and E'' is the loss modulus. Equation (8) is routinely used to calculate the dissipated energy during fatigue tests, when the specimen is being damaged[26].

Given the dependence on strain amplitude of the dissipated energy (Fig. 8a and Eq. 8), it was possible to normalize the dissipated energy also for the impulsive test carried out in this research, as follows:

$$W_n = \frac{W}{\pi\, \varepsilon_0^2} \tag{9}$$

where W_n is the normalized energy and ε_0 is the applied strain level (peak value). Fig. 9 shows the normalized energy data, for virgin curves and small-strain curves.

FIGURE 9. Energy normalized with respect to the square of the strain level: a) virgin curves; b) small-strain curves.

As was done for the values of *E*, it was possible to fit the virgin and the small-strain curves of the normalized dissipated energy using an exponential equation:

$$W_n = W_{n0} \exp(-\theta\varepsilon) \tag{10}$$

where ε is the peak of the maximum applied strain, W_{n0} is the normalized energy at "zero deformation" and θ is the slope of the curve that characterizes the strain-dependance of W_n. Table 3 shows the estimated values of $W_{n0,V}$ and $W_{n0,SS}$ for the virgin curves and for small-strain curve, their ratio, and θ_V and θ_{SS} estimated for the virgin curves and for small-strain curves, respectively. It can be highlight that, for CBTM specimens, the values of $W_{n,SS}$ were higher than the values of $W_{n,V}$, suggesting that on the damaged specimens the bituminous bonds had a higher influence on the resilient stiffness response. We hypothesize that this behavior is due the breaking of the cementitious bonds that created microcracks and reduced the effective area of the specimen, inducing damage. However, stiffness and cohesion

continued to be provided by bituminous bonds, which were more ductile (none of the specimen collapsed even if the stiffness reduced in some cases to less than 20 % of the initial value). On the contrary, for the AC mixtures, the values of $W_{n,SS}$ were lower than the values of $W_{n,V}$, suggesting a different mechanism of damage. A similar behavior was observed in fatigue test on CBTM mixtures and AC mixtures[27,28].

Comparing Equation 8 to Equation 9, even when stress and strain were not sinusoidal, we can find an energy-equivalent loss modulus $\tilde{E}''$ calculated on from the dissipated energy W:

$$\tilde{E}'' = W_n \tag{11}$$

Similarly to what reported in Section 4.2, an energy-based damage parameter $\tilde{D}$ can be defined as follows:

$$\tilde{D} = 1 - \frac{\tilde{E}''}{\tilde{E}_0''} \tag{12}$$

where $\tilde{E}''$ and $\tilde{E}_0''$ are the values of the energy-equivalent loss modulus of the damaged and undamaged specimens, respectively. Fig.10 shows the values of $\tilde{E}''/\tilde{E}_0'' = (1 - \tilde{D})$ versus the maximum strain level applied to the specimen. The curves were fitted using Equation 10 and were characterized by the same θ_{SS} listed in Tab. 3. Specifically, θ_{SS} represents the rate of damage evolution evaluated using the energy-equivalent loss modulus. The θ_{SS} values can be compared to the corresponding k_{SS} representing the rate of damage evolution evaluated using the resilient stiffness nodulus. For the CBTM specimens the ratio k_{SS}/θ_{SS} is well above one (comprised between 1.53 and 4.1) indicating that the rate of damage evolution was higher when considering the resilient response (k_{SS}) as compared to the loss response (θ_{SS}). This confirms

that the breaking of cementitious bond plays a key role for the damage evolution in CBTM mixtures.

FIGURE 10. Normalized energy-equivalent loss modulus versus maximum strain level for the small strain curves.

TABLE 3. Least-squares estimates of the parameters of Equation 10.

Specimen ID	$W_{n0,V}$ (MPa) (MPa) Virgin	$W_{n0,SS}$ Small strain	$W_{n0,V}/W_{n0,SS}$ (-)	ϑ_V (-) Virgin	ϑ_{SS} (-) Small strain
CBTM_R1_I	0.246	0.259	0.949	$3.4 \cdot 10^{-3}$	$3.0 \cdot 10^{-3}$
CBTM_R2_I	0.183	0.157	1.165	$1.7 \cdot 10^{-3}$	$1.1 \cdot 10^{-3}$
CBTM_R3_I	0.138	0.137	1.010	$1.3 \cdot 10^{-3}$	$1.3 \cdot 10^{-3}$
CBTM_R4_I	0.324	0.356	0.910	$3.5 \cdot 10^{-3}$	$2.7 \cdot 10^{-3}$
CBTM_R5_I	0.133	0.125	1.061	$1.4 \cdot 10^{-3}$	$1.2 \cdot 10^{-3}$
CBTM_R6_I	0.140	0.137	1.020	$1.6 \cdot 10^{-3}$	$1.8 \cdot 10^{-3}$
CBTM_R1_P	0.244	0.262	0.930	$2.1 \cdot 10^{-3}$	$1.1 \cdot 10^{-3}$
CBTM_R2_P	0.261	0.264	0.985	$2.7 \cdot 10^{-3}$	$1.7 \cdot 10^{-3}$
CBTM_R3_P	0.244	0.251	0.972	$2.1 \cdot 10^{-3}$	$1.6 \cdot 10^{-3}$
AC_R1_P	0.533	0.539	0.989	$3.0 \cdot 10^{-3}$	$8.0 \cdot 10^{-3}$
AC_R2_P	0.467	0.464	1.004	$3.0 \cdot 10^{-3}$	$4.0 \cdot 10^{-3}$

Conclusions

This paper describes a new strain sweep testing procedure aiming at separate reversible nonlinearity from irreversible damage effects. The procedure consists in a sequence of stiffness modulus tests performed at increasing strain levels, that induce damage in the specimen, combined with tests performed at small strain that are aimed at measuring the small-strain response. The terms virgin curve and small-strain curves were introduced to describe the results obtained from the steps of increasing strain, and the steps at small-strain, respectively. The

interpretation of the results was based on two approaches: by using the resilient stiffness modulus *E,* that can be considered a linear elastic parameter, and by using the energy-equivalent loss modulus $\tilde{E}''$, based on the calculation of the dissipated energy. The results showed that the two approaches allow to separate the effects due to nonlinearity (present only on the virgin curves) from those due to damage (represented by the small-strain curves). For all the CBTM specimens tested, the increase of strain from 43 to 322 με caused mostly damage, but the biasing effect of nonlinearity was clearly visible. Moreover, the damage evolution was almost identical for all specimens, regardless of temperature and mixture composition. On the other hand, for the AC mixture, the effect of nonlinearity was almost not visible. However, only two specimens of AC were tested.

In this research, the indirect tensile test with impulsive loading was adopted due to its simplicity. In future research, the strain-sweep testing procedure will be applied by using complex modulus (sinusoidal) tests in tension-compression mode of loading.

Acknowledgments

It is gratefully acknowledged that the deformation sweep tests on Polish mixtures were performed in a research project sponsored by Polish National Science Centre under the grant Miniatura 6, grant id. 2022/06/X/ST8/01275

References

1. B. Dołżycki and P. Jaskuła, “Review and evaluation of cold recycling with bitumen emulsion and cement for rehabilitation of old pavements,” Journal of Traffic and

Transportation Engineering (English Edition) 6, no. 4 (August 2019): 311-323, https://doi.org/10.1016/j.jtte.2019.02.002

2. M. Dal Ben and K.J. Jenkins, "Performance of cold recycling materials with foamed bitumen and increasing percentage of reclaimed asphalt pavement," Road Materials and Pavement Design 15, no. 2 (2014): 348–371, https://doi.org/10.1080/14680629.2013.872051
3. A. Graziani, C. Godenzoni, F. Cardone, and M. Bocci, "Effect of curing on the physical and mechanical properties of cold-recycled bituminous mixtures," Materials & Design 95 (5 April 2016): 358–369, https://doi.org/10.1016/j.matdes.2016.01.094
4. A.K. Kuchiishi, K. Vasconcelos, and L.L. Bariani Bernucci, "Effect of mixture composition on the mechanical behaviour of cold recycled asphalt mixtures", International Journal of Pavement Engineering 22, no. 8 (2021): 984–994, https://doi.org/10.1080/10298436.2019.1655564
5. A. Chomicz-Kowalska and J. Stepien, "Cost and eco-effective cold in-place recycled mixtures with foamed bitumen during the reconstruction of a road section under variable load bearing capacity of the subgrade," Procedia Engineering 161 (2016): 980–989, https://doi.org/10.1016/j.proeng.2016.08.837
6. B. Wacker, M. Kalantari, and M. Diekmann, "Cold Recycling in Germany—Current Experiences and Future Projects," in Proceedings of the 9th International Conference on Maintenance and Rehabilitation of Pavements—Mairepav9, ed. C. Raab (LNCE, volume 76, PA: Springer Cham, 2020), 813–823, https://doi.org/10.1007/978-3-030-48679-2_76

7. J. Lin, J. Hong, and Y. Xiao, (2017) "Dynamic characteristics of 100% cold recycled asphalt mixture using asphalt emulsion and cement", Journal of Cleaner Production 156 (10 July 2017): 337–344, https://doi.org/10.1016/j.jclepro.2017.04.065
8. J. Valentin, Z. Čížková, J. Suda, F. Batista, K. Mollenhauer, and D. Simnofske, "Stiffness Characterization of Cold Recycled Mixtures," Transportation Research Procedia 14 (2016): 758–767, https://doi.org/10.1016/j.trpro.2016.05.065
9. C. Mignini, F. Cardone, and A. Graziani, "Complex modulus of cement-bitumen treated materials produced with different reclaimed asphalt gradations," Materials and Structures 55 (2022): 169, https://doi.org/10.1617/s11527-022-02009-4
10. B. Dolzycki, C. Szydlowski, and M. Jaczewski, "The influence of combination of binding agents on fatigue properties of deep cold in-place recycled mixtures in Indirect Tensile Fatigue Test (ITFT)," Construction and Building Materials 239 (10 April 2020): 117825, https://doi.org/10.1016/j.conbuildmat.2019.117825
11. H. Cheng, L. Sun, L. Liu, and H. Li, "Fatigue characteristics of in-service cold recycling mixture with asphalt emulsion and HMA mixture," Construction and Building Materials 192 (20 December 2018): 704-714, https://doi.org/10.1016/j.conbuildmat.2018.10.171
12. M. Jaczewski, C. Szydłowski, and B. Dołżycki, "Stiffness of cold-recycled mixtures under variable deformation conditions in the IT-CY test," Case Studies in Construction Materials 18 (July 2023): e02066, https://doi.org/10.1016/j.cscm.2023.e02066
13. G.D. Airey, B. Rahimzadeh, and A.C. Collop, "Linear Viscoelastic Limits of Bituminous Binders," Journal Of The Association Of Asphalt Paving Technologists 71 (2002): 160-196

14. M. Jaczewski, C. Szydlowski, and B. Dolzycki, "Preliminary study of linear viscoelasticity limits of cold recycled mixtures determined in Simple Performance Tester (SPT)," Construction and Building Materials 357 (28 November 2022): 129432, https://doi.org/10.1016/j.conbuildmat.2022.129432

15. M. Jaczewski and A. Graziani, "Strain-dependent behaviour of cold recycled material mixtures in cyclic compression tests," Materials and Structures 57 (2024): 92, https://doi.org/ /10.1617/s11527-024-02366-2

16. Q.T. Nguyen, H. Di Benedetto, and C. Sauzéat, "Linear and nonlinear viscoelastic behaviour of bituminous mixtures," Materials and Structures 48 (2015): 2339-2351, https://doi.org/10.1617/s11527-014-0316-5

17. R.P. Coutinho, L.F.A.L. Babadopulos, R.A. Freire, V.T.F. Castelo Branco, and J.B. Soares, "The use of stress sweep tests for asphalt mixtures nonlinear viscoelastic and fatigue damage responses identification," Materials and Structures 47 (2014): 895-909, https://doi.org/10.1617/s11527-013-0101-x

18. C. Hintz, R. Velasquez, C. Johnson and H. Bahia, "Modification and validation of linear amplitude sweep test for binder fatigue specification". Transportation Research Record, 2207 (2011), 99-106, https://doi.org/10.3141/2207-13

19. F. E. Pérez Jiménez, R. Botella Nieto, A.H. Martínez Reguero, and J.R. Miró Recasens, "Estimating the fatigue law of asphalt mixtures using a strain sweep test (EBADE test)," In Proceedings of the 5th International EATA Conference, Braunschweig, Germany (2013).

20. R. Botella, F.E. Pérez-Jiménez, R. Miro and A.H. Martínez, "New methodology to estimate the fatigue behavior of bituminous mixtures using a strain sweep test,"

Construction and Building Materials, 135 (2017), 233-240, http://dx.doi.org/10.1016/j.conbuildmat.2016.12.190

21. I. Isailović and M.P. Wistuba, "Sweep test protocol for fatigue evaluation of asphalt mixtures," Road Materials and Pavement Design, 20 n. 5 (2019), 1131-1144, https://doi.org/10.1080/14680629.2018.1438305
22. M. Kalantari, "Foamed Bitumen and Cement Stabilized Mixes – Characterisitics and Pavement Design," PhD Dissertation, School of Science and Technology of the University of Siegen, Siegen, Germany, 2022, http://dx.doi.org/10.25819/ubsi/10082.
23. M. Kalantari, "Cold recycling with foamed bitumen, gained knowledge from a test track in Germany," Roads & Bridges/Drogi i Mosty, Vol. 22 No. 4 (2023), https://doi.org/10.7409/RABDIM.023.028.
24. L. Babadopulos, G. Orozco, S. Mangiafico, C. Sauzéat, and H. Di Benedetto, "Influence of loading amplitude on viscoelastic properties of bitumen, mastic and bituminous mixtures," Road Materials and Pavement Design 20, no. sup2 (2019): S780-S796, https://doi.org/10.1080/14680629.2019.1628428
25. H. Di Benedetto, C. De La Roche, H. Baaj, A. Pronk, and R. Lundström, "Fatigue of bituminous mixtures," Materials and Structures 37 (2004): 202-216, https://doi.org/10.1007/BF02481620
26. A.A. Tayebali, G.M. Rowe, and J.B. Sousa, "Fatigue response of asphalt-aggregate mixtures (with discussion)," Journal of the Association of Asphalt Paving Technologists 61 (1992): 333-360
27. V. Grilli, A. Virgili, and A. Graziani, "Evaluation of complex modulus and fatigue properties of cold recycled material mixtures using small-scale specimens," Road

Materials and Pavement Design 25, no. 1 (2024): 115-130, https://doi.org/10.1080/14680629.2023.2194450

28. A. Graziani, S. Spadoni, L.P. Ingrassia, A. Virgili, and F. Canestrari, "Composite fatigue failure of cold recycled material mixtures: new insights into the role of bitumen and cement. Materials and Structures 57 (2024): 10, https://doi.org/10.1617/s11527-023-02285-8

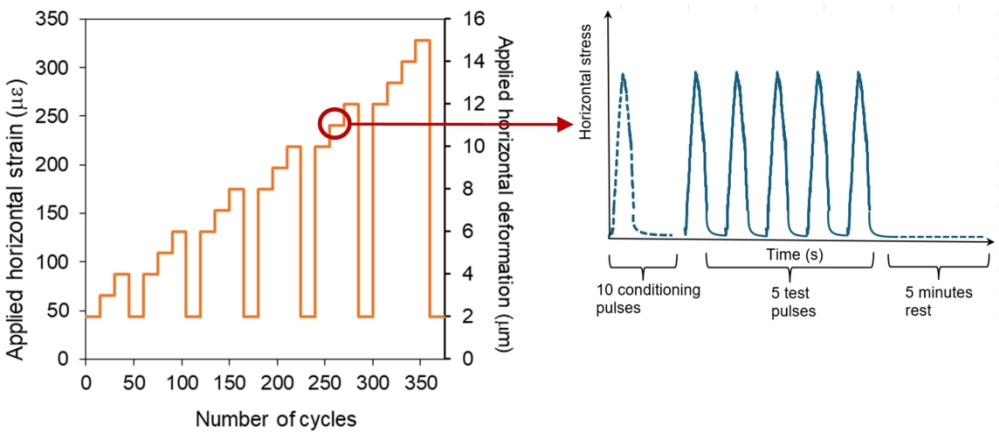

Figure 1. Deformation and strain levels applied to the specimens and test pulses.

332x166mm (300 x 300 DPI)

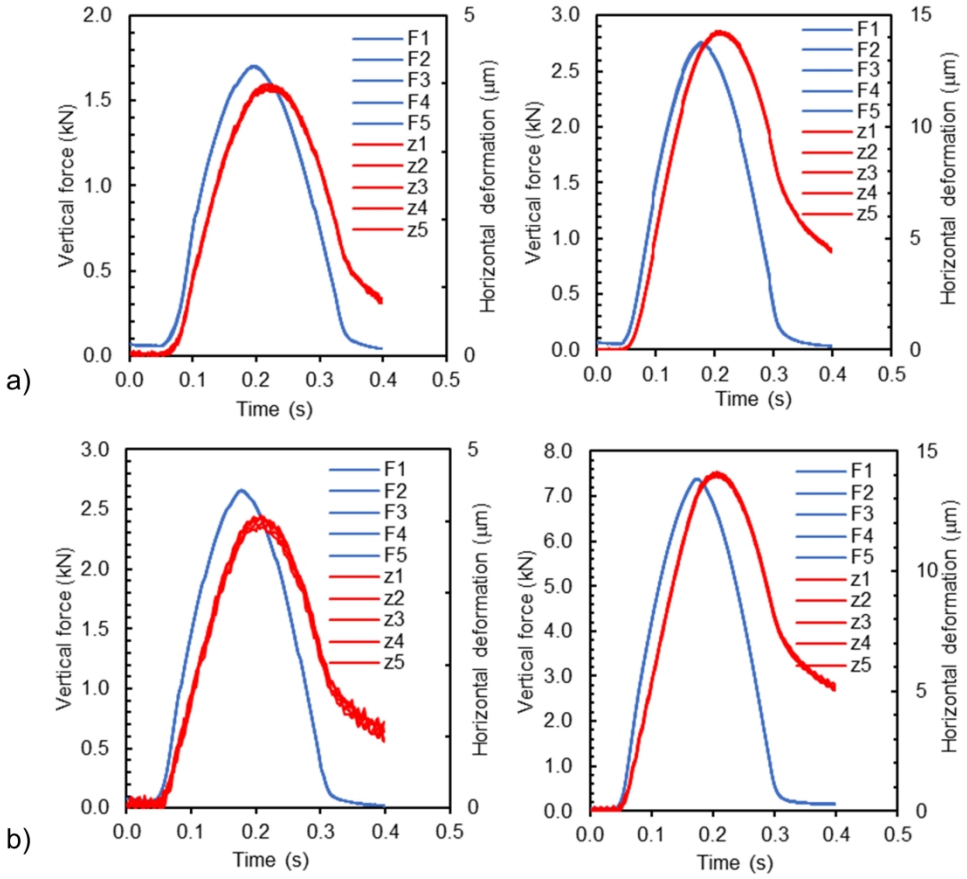

Figure 2. Time-histories of five test pulses of vertical force and horizontal deformation, recorded on two specimens at target horizontal deformations of 4 μm and 14 μm; a) specimen CBTM_R3_P; b) specimen AC_R1_P.

353x353mm (300 x 300 DPI)

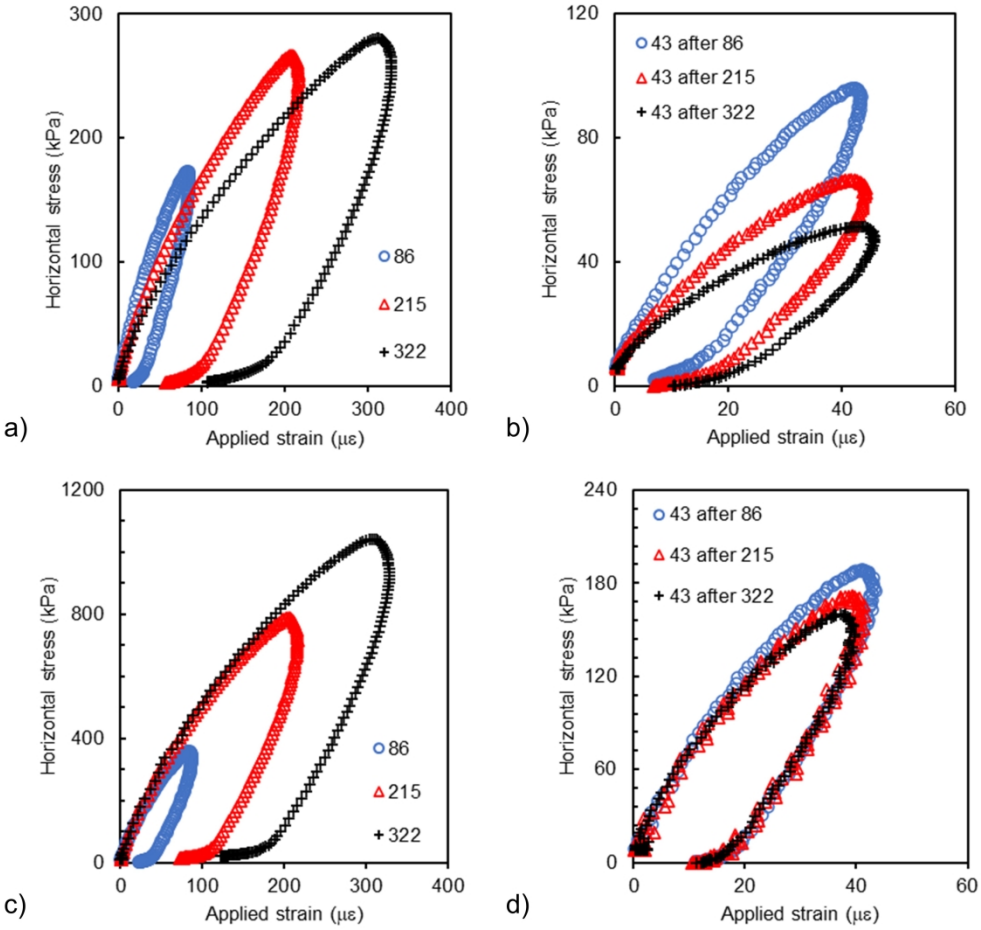

Figure 3. Lissajous plots (stress vs strain) recorded at large and small strain: a) specimen CBTM_R3_P from 86 to 322 με; b) specimen CBTM_R3_P 43 με; c) specimen AC_R1_P from 86 to 322 με; d) specimen AC_R1_P 43 με.

370x370mm (300 x 300 DPI)

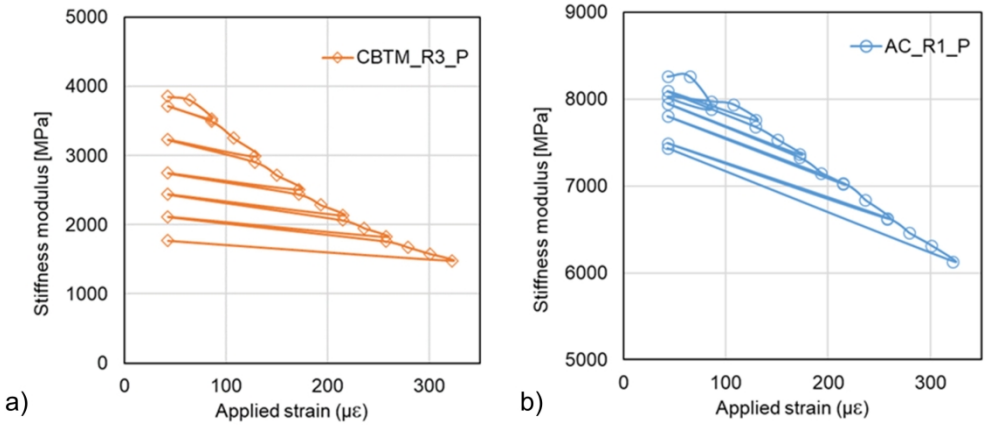

Figure 4. Resilient stiffness modulus measured in the strain sweep tests; a) specimen CBTM_R3_P; b) specimen AC_R1_P.

377x188mm (300 x 300 DPI)

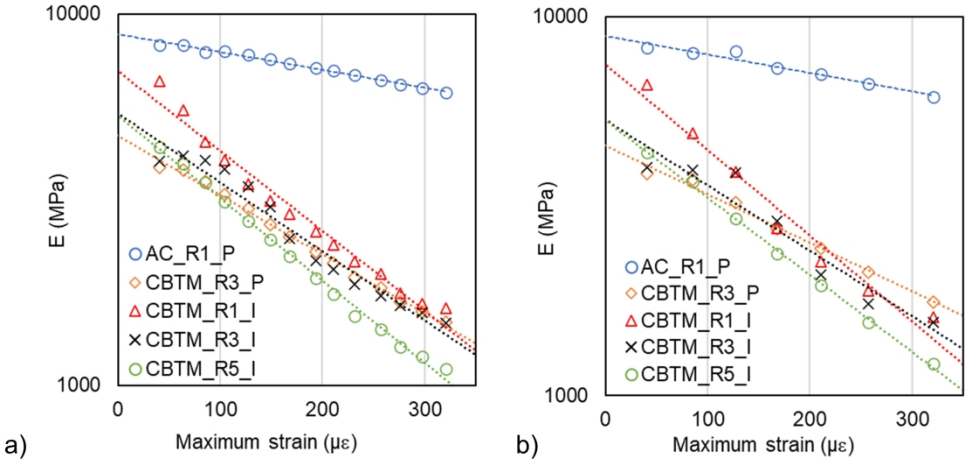

Figura 5. Resilient stiffness modulus variation as a function of applied strain level: a) virgin curve; b) small-strain curve.

493x246mm (300 x 300 DPI)

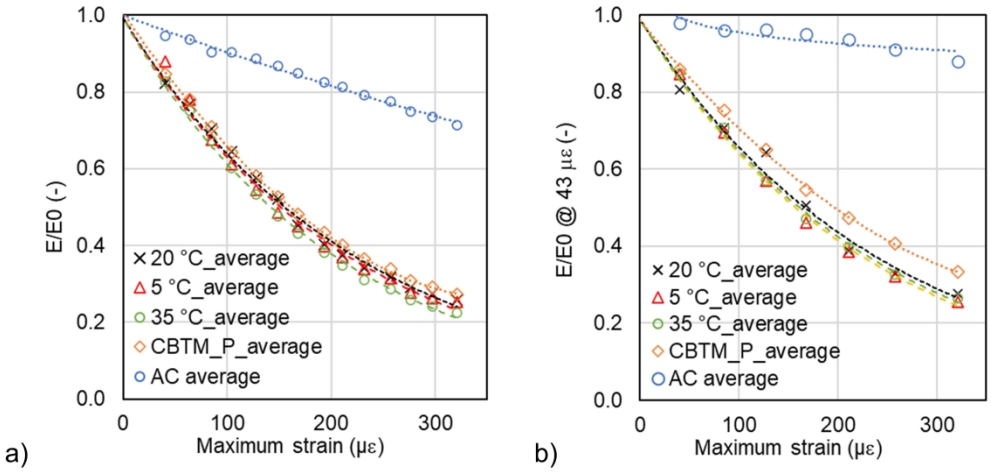

Figure 6. Normalized stiffness modulus versus maximum strain level: a) virgin curves; b) small-strain curves

477x238mm (300 x 300 DPI)

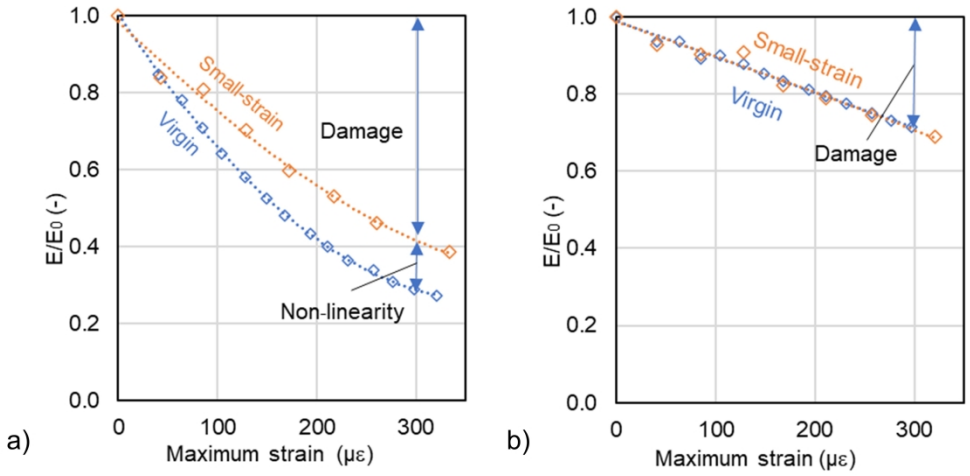

Figure 7. Virgin and small-strain curves. a) specimen CBTM_R3_P; b) specimen AC_R1_P.

405x190mm (300 x 300 DPI)

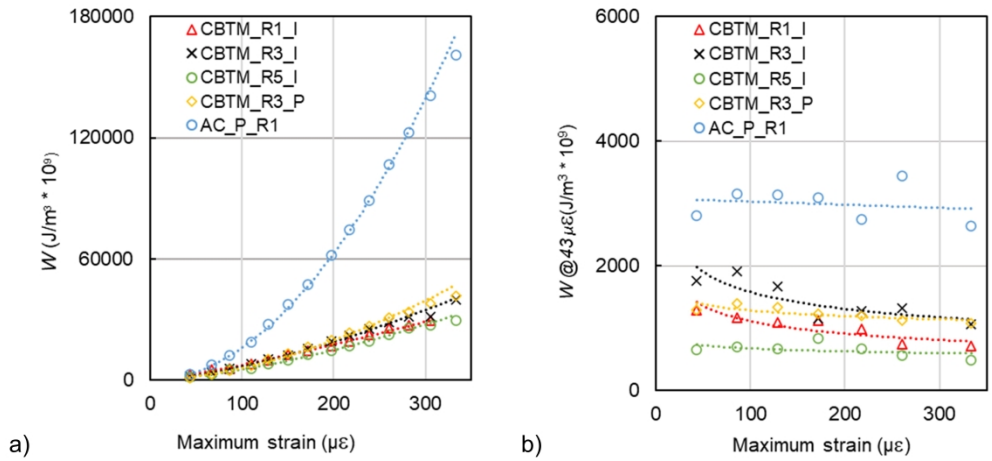

Figure 8. Dissipated energy per volume, per cycle: a) virgin curves; b) small-strain curves.

459x210mm (300 x 300 DPI)

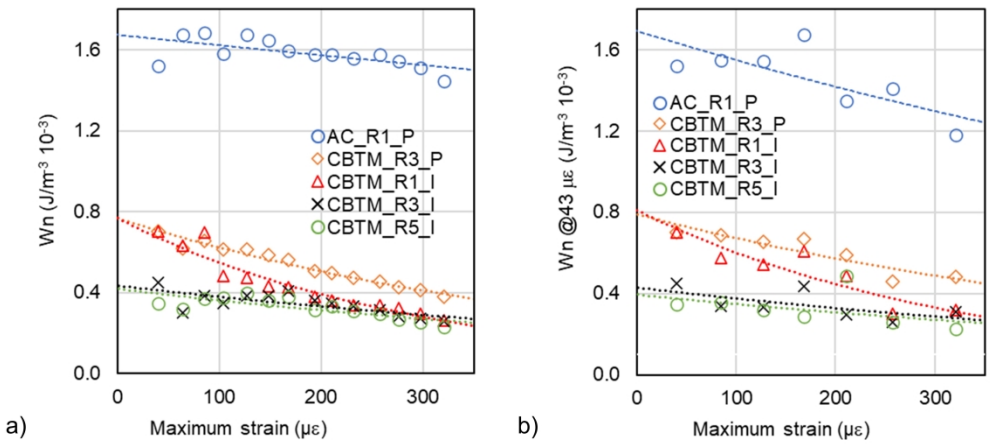

Figure 9. Dissipated energy normalized with respect to the square of the strain level: a) virgin curves; b) small-strain curves.

458x205mm (300 x 300 DPI)

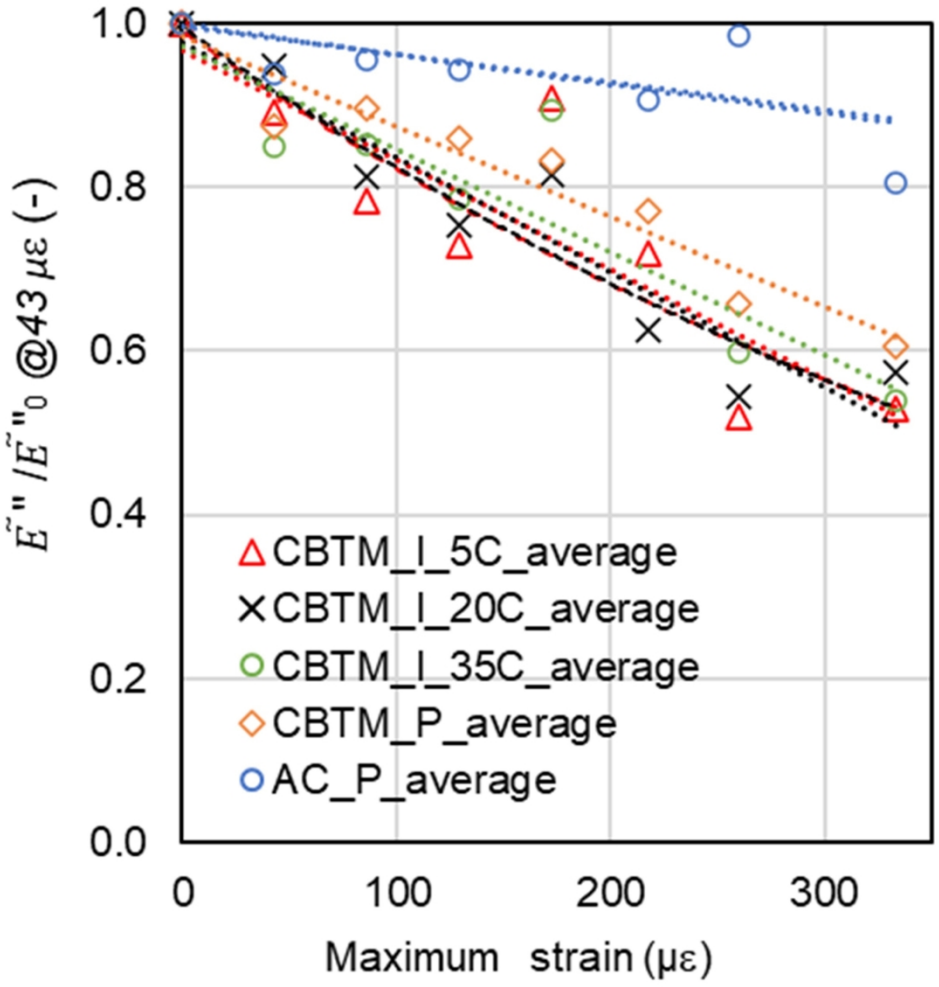

Figure 10. Normalized energy-equivalent loss modulus versus maximum strain level for the small strain curves.

215x215mm (300 x 300 DPI)